Clean Energy, 2023, Vol. 7, No. 3, 509–518
https://doi.org/10.1093/ce/zkac068
Advance access publication 6 May 2023
Research Article

Design of a new static solar concentrator with a high concentration ratio and a large acceptance angle based on bifacial solar cells

Adnan Shariah* and Emad Hasan

Physics Department, Jordan University of Science and Technology, PO Box 3030, Irbid, Jordan
*Corresponding author. E-mail: shariah@just.edu.jo

Abstract

Solar concentrators are used in solar photovoltaic systems to lower the cost of producing electricity. In this situation, fewer solar cells can be used, lowering the overall cost of the system. The purpose of this article is to design, construct, install and test a stationary (non-tracking) concentrating system in Irbid, Jordan. Bifacial solar cells are used in the design. Two concentrator designs (with the same concentration ratio) are experimentally tested. Conc-A has a parabolic shape in the lower part but flat reflecting walls, whereas Conc-B has a standard compound parabolic shape in all parts. The receiving solar cells are arranged in three distinct positions in each concentrator. The results reveal that the output power from both concentrators is affected by the placement of the receiving solar cells within the concentrator. It has also been found that concentrators with flat reflecting walls perform better than those with parabolic reflecting walls. Conc-A's power collection is ~198% greater than that of a non-concentrating device. When Conc-B is used, the increase in power is ~181%.

Graphical Abstract

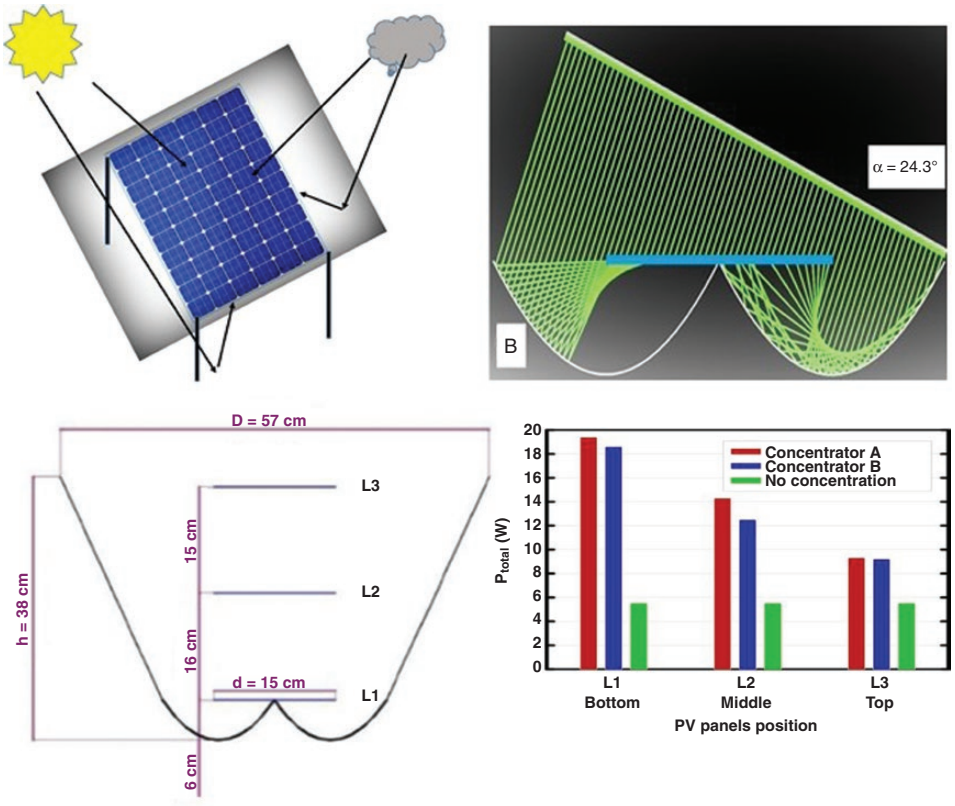

Keywords: bifacial solar cell; non-tracking system; parabolic trough concentration; PV concentrators

Received: 25 June 2022. **Accepted:** 15 November 2022

Introduction

Electricity is one of the most crucial components of the Industrial Revolution. The daily demand for energy is rising as a result of the improving living standards of societies and the continuing growth of the population. This has led scholars and scientists to seek more economical, less-polluting and more efficient energy alternatives [1]. Solar energy is the primary alternative energy source since it is one of the most abundant alternative energy sources and will be available for a very long period. Solar technologies include photovoltaic (PV) panels, which convert sunlight directly into electricity, and solar concentrators, which turn sunlight directly into thermal energy. In the past two decades, technological advances have reduced the price of PV panels and increased their efficiency, resulting in a focus on solar energy. New technological advances are expected to boost the use of PV systems by reducing the cost and increasing the efficiency of solar panels [2–4]. Perovskite solar cells [5], heterojunction technology [6], integrated PV cells in buildings [7], printable solar cells [8], bifacial cells, thin wafers and thin-film solar cells are among the new breakthroughs. Researchers are motivated to improve concentrated photovoltaic (CPV) technology employing commercially available bifacial solar modules in an effort to further drop prices and increase efficiency [9].

PV concentrators utilize lenses or mirrors to focus the Sun's rays on the solar cells. CPV systems have several advantages over non-concentrating PV systems since they may gather the same amount of radiation, if not more, with fewer solar cells. The disadvantage of the CPV is a rise in temperature, so it is essential to dissipate the heat generated by the PV cells.

Low-concentrating PV (LCPV) systems rely on fixed reflectors and receivers (called static concentrators), whereas high-concentrating PV (HCPV) systems and medium-concentrating PV (MCPV) systems rely on movable reflectors and/or receivers. The second and third types of concentrators acquire precision tracking to maintain the Sun's light concentrated on the solar cells during the day, increasing the system's cost, complexity and maintenance load [10].

The high acceptance angle of static concentrators eliminates the need for Sun tracking and enables the concentration of both diffuse and direct radiation. They have been the focus of numerous studies for many years. The most prevalent LCPV concentrator geometries are paraboloid (symmetric, asymmetric, and truncated) and V-trough. In recent years, it has been the topic of various studies and a number of great review articles [11–17] have been published in the field.

For example, Parupudi *et al.* [18] examined three LCPV designs with one-sided solar cells, including asymmetric compound parabolic concentrating (ACPC), compound parabolic concentrating (CPC) and V-trough optical concentrators with geometric concentration ratios of 1.53, 1.46 and 1.40, respectively, and according to their measurements, the ACPC concentrator had the highest annual optical efficiency. Experimentally, Alnajideen and Gao [19] examined a new design consisting of two standard V-trough concentrators placed in a cross. The results indicated that the concentration ratio of this new structure is 40–60% higher than its typical V-trough solar concentrator counterpart. Butlers *et al.* [20] used a modified V-trough concentrator, combined with a heat-sink apparatus, utilizing the fact that LCPV has the ability to capture more energy than conventional Si solar cells in a basic concentration configuration.

In parabolic trough concentrators, a parabolic-shaped mirror focuses sunlight on a receiver tube at the focal point of the parabola [21]. Mallick *et al.* [22] developed an asymmetric CPC that did not require imaging. Their experiments revealed a 62% improvement in maximum power output when compared to a comparable non-concentrating PV panel. Mokri [23] performed experiments on CPV technology and its economic potential, as well as the potential for this technology to bring the cost of energy to a level comparable to that of oil-based resources.

Solar concentrators have also been used in hybrid electric/thermal systems (PVT), such as [24] and [25], where both electric energy and heat could be obtained from the system. Masood *et al.* [26] gave a comprehensive review of the applications of CPCs in hybrid PVT systems. Katardjiev [27] introduced a novel method to concentrate both direct and indirect sunlight by combining waveguiding and refractive optics. The design displayed a transmittance of >90% at acceptance angles of <65° at 3 suns for moderate refractive indices. In addition to PV conversion, the new method harvested waste heat to maximize the use of solar radiation, achieving an energy efficiency for diffuse light of >70%.

Bifacial solar panels are a new product in the PV industry that have just recently become commercially available. When used as conventional solar panels, the power output can be increased by ≤30% depending on the kind of ground (concrete, green field, white gravel, sand, etc.), the height of the installation and the tilt angle of the panels [28–31]. Because such panels receive solar radiation from both sides, developers could design solar PV concentrators that reflect solar energy onto both sides of the solar cell.

Rabl [32] presented the first concentrator of this type to be used in the building-integrated PV system Fig. 1. There are just a few research studies on the design of low ratio static solar concentrators that employ bifacial PV silicon solar cells. For example, Chacin *et al.* [33] computationally and experimentally investigated two CPCs. Each had a distinct concentration factor (1.25 and 1.66) and was outfitted with bifacial cell receivers that were vertically positioned. Higher concentration factors meant higher operating temperatures (for closed collectors with a top glass cover) (114°C for a concentration factor of 1.66 and 96°C for a concentration factor of 1.25). The observed concentration ratios were low—less than half of the desired values for both receivers. They attributed the difference to an increase in the temperature of the panel. Panchal *et al.* [34] simulated and experimentally tested two concentrating photovoltaic thermal (CPVT) system designs. The collectors used a pure parabolic and a compound parabolic reflector design, with concentration factors of 1.2 and 1.6, respectively. Their concentrator was designed using Tonatiuh ray-tracing software. The results of the field tests (measured at solar noon and the best incidence angle) showed that pure parabolic was more

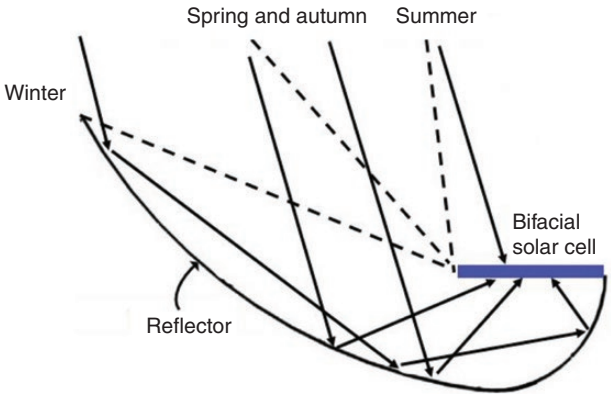

Fig. 1: Schematic diagram of sea shell concentrator.

effective than compound parabolic. Poulek *et al.* [35] designed and tested tracking PV pseudo parabolic concentrators using bifacial solar panels with silicone gel laminated on both sides. Daily energy gains of ≤167% were measured and the summer working temperature of PV panels was +95°C. Aghaei *et al.* [36] investigated the optical and electrical performance of a 1-cm^3 mosaic cubical luminescent solar concentrator by miniaturizing cubical light guides and mounting bifacial solar cells to the edges of neighbouring light guides. The maximum power-conversion efficiency was found to be 11.6%. Consequently, there is a lack of research on static low ratio PV concentrators that utilize bifacial solar cells.

1 Design parameters for LCPV concentrators

The compound parabolic concentrator and V-trough solar concentrator are the two main shapes utilized to manufacture LCPV solar concentrators for conventional monofacial silicon solar cells, in addition to their asymmetrical and truncated shapes. Typically, the concentration ratio characterizes the light-concentration process. The most common definition of a concentration ratio (CR) is the ratio between the aperture area and the receiver area. This is called the geometric concentration ratio (C_g). When coupled with the reflectivity of the surface, it is referred to as the effective concentration ratio (C_{eff}). LCPV concentrators can reflect all incident radiation to the receiver over large ranges of incidence angle. Limits specify the concentrator acceptance angle (θ). All radiation within the acceptance angle is reflected to the receiver. Fig. 2 illustrates the structure of a typical V-shaped and paraboloid LCPV concentrator and the relevance of the acceptance angle limit. The same definition can be used for compound parabolic concentrators.

Geometric and effective CR can be expressed as follows [37]:

$$C_g = \frac{A_a}{A_r} = 1 + 2\cos\Phi \tag{1}$$

$$C_{eff} = R\ C_g \geq 1 + 2R\cos\Phi \tag{2}$$

In this instance, R represents the reflectance of the reflector, L is its length, Φ is the vertex angle, and A_a and A_r represent the aperture and absorber areas, respectively.

The acceptance angle (θ) is one of the most crucial parameters in solar concentrators. It is defined as the maximum angle at which the receiver can capture incoming sunlight. The equation below describes the link between the geometrical concentration ratio (C_g) and the acceptance angle [38]:

$$C_g = \frac{1}{\sin\theta} \tag{3}$$

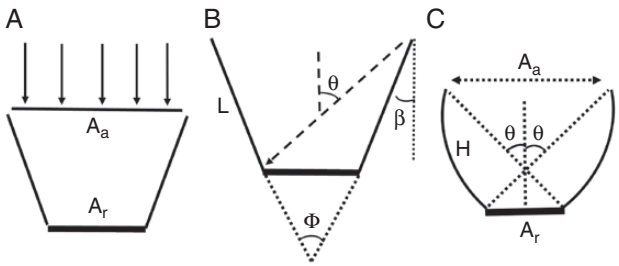

Fig. 2: Schematic diagram of a typical V-shaped and paraboloid LCPV concentrator.

The CR is sometimes denoted by the optical concentration ratio (C_{opt}) and is defined as the average irradiance (radiant flux, I_r) integrated over the receiver area (A_r) divided by the incident insolation on the collector aperture (I_a). The mathematical form of this expression is [39]:

$$C_{opt} = \frac{\frac{1}{A_r}\int I_r\, dA_r}{I_a} \tag{4}$$

The optical efficiency is given by [40]:

$$\eta_{opt} = \frac{C_{eff}}{C_g} \tag{5}$$

2 Methodology

2.2 Design procedure

Our goal was to build an LCPV concentrator with the highest possible concentrating value, the largest possible acceptance angle and an area (rectangular shape) of ray concentration as opposed to a line. We began with a V-shaped concentrator and tracing the rays that fall onto it reveals the pattern depicted in Fig. 3. It is well known that rays striking a reflector with an incidence angle of less than θ will be reflected towards the receiver (green arrows). Those falling at a greater angle than θ will miss the receiver and be reflected away by the second reflector (red arrow).

To increase the CR, the aperture area of the concentrator must be increased (while the area of the receiver remains unchanged). This can be accomplished by extending the distance between the tops of the two reflectors or by distancing the reflectors. Fig. 4 displays

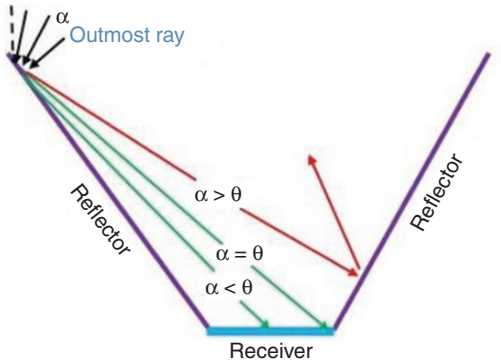

Fig. 3: Ray-tracing falls at various incidence angles on a V-shaped concentrator.

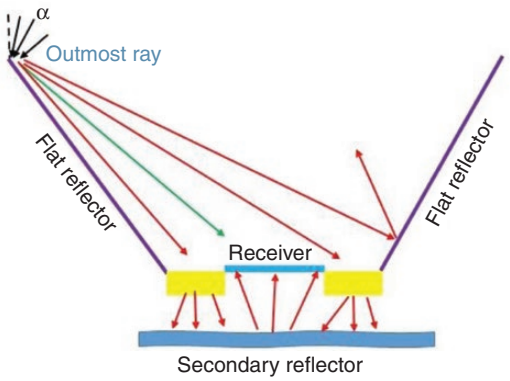

Fig. 4: When reflectors are separated, ray-tracing falls at varying incidence angles on a V-shaped concentrator.

the pattern of the reflector's reflected rays (extreme rays). Evidently, some of the rays reflected towards the concentrator's bottom will miss the receiver and escape the concentrator (yellow regions).

Our hypothesis is that it is possible to put a second reflector of a specific shape beneath the yellow parts so that it can reflect the rays that escape from these areas back towards the rear of the receiver (bifacial solar cell in this case). We used a ray-tracing program to verify the hypothesis.

2.2 Ray-tracing analysis

The concentrator was designed using Ray Optics Simulation Software [41]. The program simulates a wide range of optical phenomena using models of up to three-dimensions. It takes into account light's absorption, specular reflection and refraction, scattering and aperture diffraction. It is supplied with a range of ray reflectors, which the user can modify using the cursor. It facilitates the design of complex and precise reflector shapes. We used the ray-tracing method to test various shapes, including flat and/or curved ones, as well as single or multiple ones, in a variety of positions, in order to find the most effective configuration that can be used as a secondary reflector to reflect the rays to the back side of the receiver. As a result, we found that two wide parabolic shapes arranged side by side, with the receiver placed on top and covering half of the aperture area of each, will be sufficient to satisfy the need. This configuration can be seen in Fig. 5. This concentrating structure has been used previously in concentrated solar-thermal systems (the receiver in these systems is a flat-plate solar collector) [42, 43] and more recently in concentrated solar PV and thermal systems (with bifacial PVT horizontal receiver) [44, 45] and concentrated solar PV and thermal systems (with bifacial PVT vertical receiver) [34].

As shown in Fig. 5a, when the incident angle is zero, all rays strike the absorber's upper surface normally and uniformly. Although it receives the back surface at varying angles (mainly normal), only a small number of rays receive it at large angles. Since a curved mirror reflects light, it is noticeable that light rays reaching the back surface are not uniform.

When the incident angle of the falling rays increases from zero, the rays reflected by the two parabolas follow distinct patterns. While the parabola closest to the light source (the one on the right) still scatters the reflected rays on the rear surface, the parabola on the left focuses the reflected rays near the far end of the receiver. Fig. 5b illustrates the scattered rays for an incident angle of 24.3°. When the incident angle of the rays is increased further, a portion of the rays reflected from the left parabola will miss the receiver and disperse. Fig. 5c shows that when the incidence angle approaches 36°, all rays reflected from that reflector are scattered away from the receiver. The acceptance angle for the parabola on the right and the receiver is (theoretically) 90°, but the acceptance angle for the parabola on the left is between 24° and 36°.

Fig. 6 depicts the resulting concentrators when the aforementioned concentrator is paired with the concentrator including V-shaped or parabolic reflectors. Therefore, the optimal concentrator design has been basically determined. Fig. 7 shows the schematic diagram of the proposed concentrators. Each of these has a length of 60 cm and an acceptance angle of 62.6° for a concentrator of a flat side reflector (Conc-A) and of angle 56.3° for a concentrator of a paraboloid side reflector (Conc-B).

2.3 Receiver specifications

The receiver consists of two independent sets of solar cells (no connection between them) connected back to back. Each group comprises four series-connected monofacial polysilicon solar cells. The purchased cells have the following specifications: P_{max} = 3.99 W, V_{OC} = 0.621 V, I_{SC} = 8.203 A, FF = 78.3%, η = 16.4%, temperature coefficient of (P_{max}) = –0.45% and busbars number = 3. When the receiver is put in the concentrator, two distinct groups of data are recorded: one group corresponds to the solar cells at the top, while the other group corresponds to the solar cells at the back. In our physics department's Solar Energy Lab, we connect and assemble the solar cells that make up the receiver. Fig. 8 displays the receiver schematic diagram.

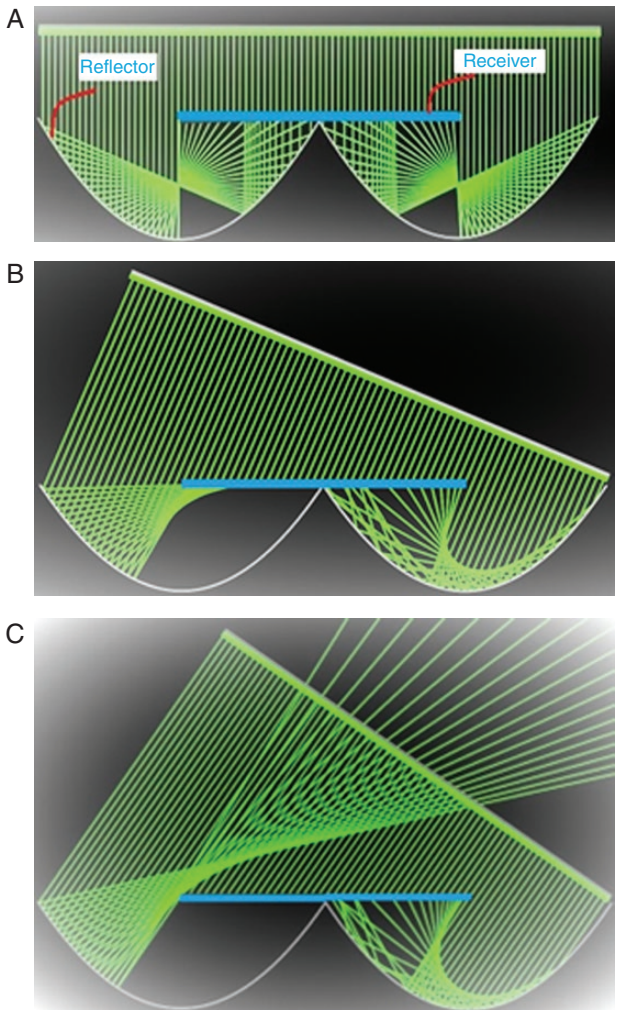

Fig. 5: Ray-tracing falls at varying incidence angles on two parabolic-shaped reflectors arranged next to one another, with the receiver positioned on top.

2.4 Manufacturing the prototype

In a workshop at the Industrial Zone of Irbid city, 1-mm-thick galvanized iron sheets are used to construct the concentrator walls. Conc-A is constructed by truncating the inner walls of two parabolas at the fixed point, followed by fusing them at the cut point. Two flat reflectors measuring 60 cm in length and 57 cm in width are fitted. Conc-B has the same dimensions as Conc-A, but its reflectors are compound trough parabolas, as illustrated in Fig. 9. Each concentrator features three receiver locations, designated L1, L2 and L3. These locations are used to identify the optimal placement of the solar panel within the concentrator to maximize power output. Self-adhesive reflector (mirror) film with 85% reflectivity is applied on galvanized sheets.

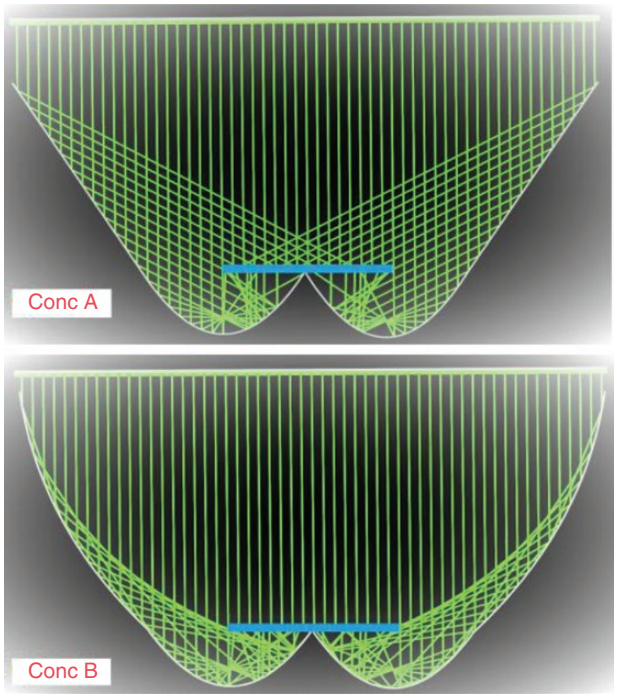

Fig. 6: Normal incident ray tracing of the proposed concentrators.

2.5 Experimental procedure

The stationary concentrators' longitudinal axis is aligned east–west and the surface is tilted 32° due south (location geographical coordinates; 32.5° N, 36° E). The concentrators are installed on the roof of the PH4 building at Jordan University of Science and Technology, as depicted in Fig. 9. The top (or bottom) module is linked to a variable resistor, a voltmeter is connected in parallel with the resistor and an ammeter is connected in series with the resistor. The resistance ranges from zero to a very high value and the voltages across the resistor and the current are recorded for each resistance value. Data for Levels L1, L2 and L3 were recorded on 17, 18 and 19 October 2018, respectively. Measurements were made at 1-h intervals between 8:00 a.m. and 4:00 p.m. on days with clear skies. Both concentrators used the same receiver to ensure that the tests were carried out under identical conditions. Similarly, data were recorded for the module while it was outside of the concentrator. The recorded data were then evaluated using current vs voltage (*I*–*V*) and power vs voltage (*P*–*V*) curve diagrams. When a curve is plotted, curve fitting is performed. The following figures include the plotted data.

3 Results and discussion

The performance of a CPV system is measured by analysing the solar panel's output current, voltage and power at various times of the day. The *I*–*V* and *P*–*V* curves for Conc-A and Conc-B are shown in Figs 10 and 11, respectively. The receiver was placed on the concentrator's lowest level (L1) and data were collected at 8:00 a.m. on 17 October 2018. Clearly, the top panel generates more open-circuit current (I_{sc}) and maximum power (P_{mp}) (I_{sc} = 6.6 A and P_{mp} = 7.8 W) than the back panel (I_{sc} = 1.6 A and P_{mp} = 1.9 W). This is due to the fact that the top panel receives more radiation than the back one, i.e. direct radiation and radiation reflected from the upper portion of the reflector walls. Although the panel on the back side receives only part of the radiation reflected from the concentrator's walls (the lower part of the walls), the output values for a similar

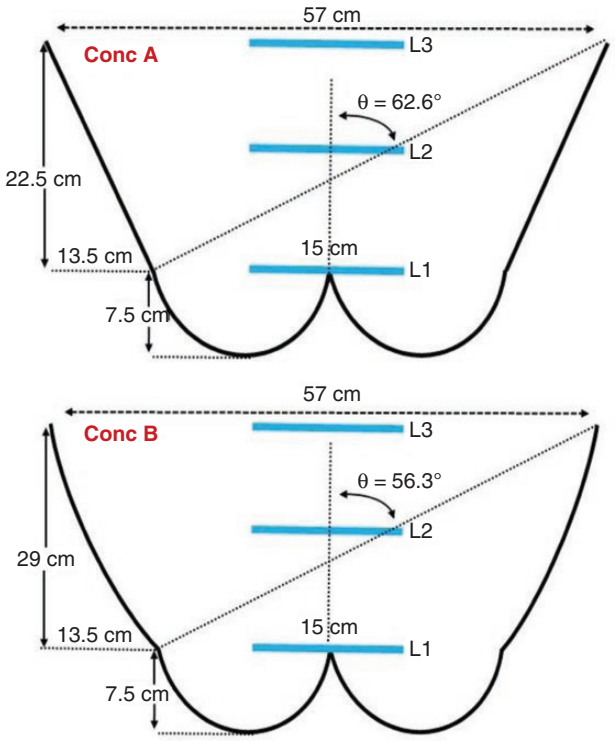

Fig. 7: Schematic illustration of the concentrators' dimensions, receiver locations and acceptance angles.

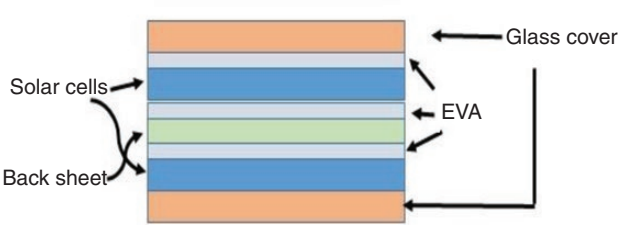

Fig. 8: Schematic illustration of solar panels serving as a receiver.

Fig. 9: Photo of installed concentrators.

panel without concentration were I_{sc} = 3 A and P_{mp} = 3.1 W. It is clear that the output of the back panel is lower than that of the panel without concentration, which indicates that this panel receives radiation from less than one sun. The I_{sc} and P_{mp} values for the top panel are much higher than those for the back panel (~1.4 A and ~1.5 W) and the output of the back panel is lower than that of the panel without concentration. This is also true for Conc-B. As time passes through the day, towards noon, the solar radiation intensity increases and hence the output of the three panels (Conc-A, Conc-B and the one without concentration) increases, too. At 10:00 a.m.

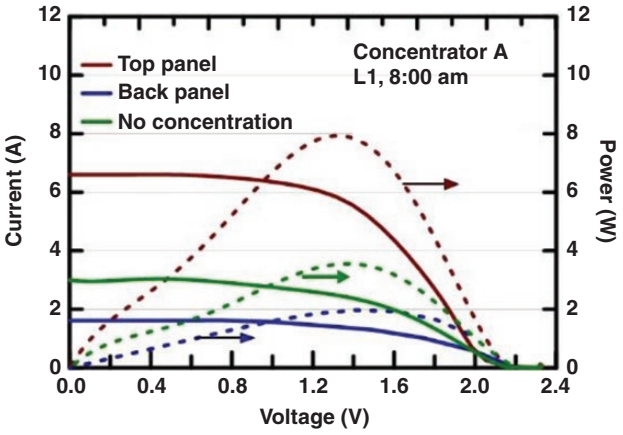

Fig. 10: *I–V* and *P–V* curves for Conc-A, L1.

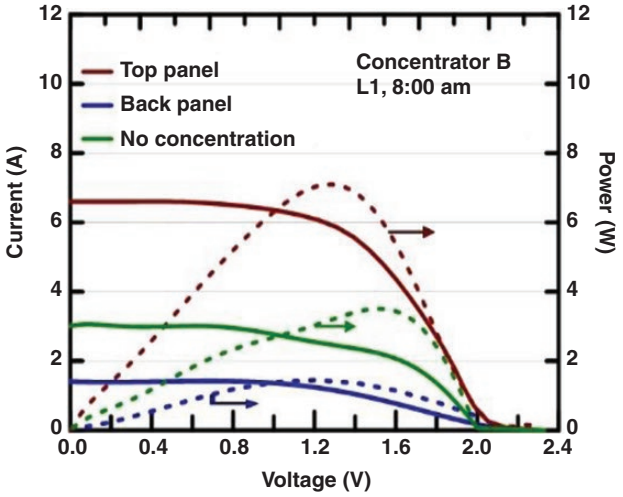

Fig. 11: *I–V* and *P–V* curves for Conc-B, L1.

(after 2 h), the scenario, qualitatively, is similar to that collected at 8:00 a.m., where the top panel generates more power and current than the other panels. When the total output power generated at 10:00 a.m. by the two concentrators and the panel without concentration (power for Conc-A and Conc-B is the sum of power generated by the top panel and the back panel) is compared to the total output power generated by the same systems at 8:00 a.m., one can observe that the total power generated by Conc-A increased by ~42% and the increase was ~21% for Conc-B and ~45% for the panel without concentration. The fact that the increase in the total output power of panels in Conc-B is low may be attributed to the statement that, as the time approaches noon, the reflected radiation from the upper part of the walls misses largely the surface of the top panel. At this time of the day (10:00 a.m.), Conc-A performs better than Conc-B by ~29% and the effective CR is ~3.1, which is the same as that at 8:00 a.m. The *I–V* and *P–V* curves for all panels at solar noon are depicted in Figs 12 and 13, respectively. Because the intensity of solar radiation reaches its maximum value of the day, the total power collected by all solar panels also reaches its maximum value. Also, at this time of the day, Conc-A performs better than Conc-B only by ~4%, with C_{eff} of ~3.1.

The relative increase in the total power from the three systems (Conc-A, Conc-B and panel without concentration) at noon, in comparison to that at 10:00 a.m., is ~41%, ~79% and ~22%, respectively. Also, at this time of day, Conc-A performs better than

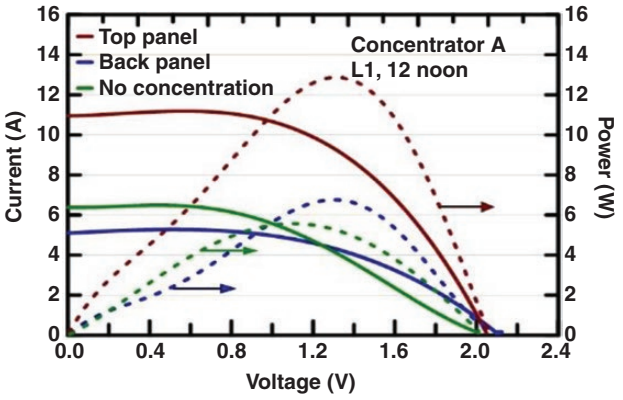

Fig. 12: *I–V* and *P–V* curves for Conc-A, L1, 12:00 noon, 17 October 2018.

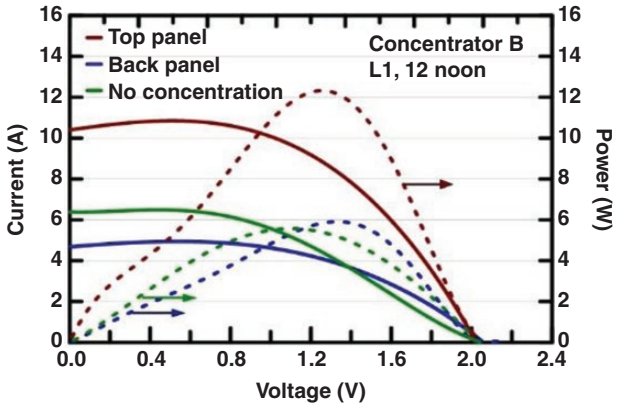

Fig. 13: *I–V* and *P–V* curves for Conc-B, L1, 12:00 noon, 17 October 2018.

Conc-B by ~4% and the C_{eff} is ~3.1. The relative increases in the total power by the three systems (Conc-A, Conc-B and panel without concentration) at noon compared to those at 10:00 a.m. are ~41%, ~79% and ~22%, respectively.

Under all circumstances, the output from panels collected during afternoon periods is identical in amount and behaviour to the results obtained from panels collected during the corresponding times before noon. To avoid duplication, the results of the data collected at 2:00 p.m. and 4:00 p.m. are not presented here. The above measurements are repeated for the case in which the receiver panels are located at Level L2 (at the middle height of the concentrator). The output power and current for all panels are shown in Fig. 14 for Conc-A and in Fig. 15 for Conc-B. Here, it is observed that panels (top and back panels) in both concentrators are operated with less output power and current compared to their output values when they are located at Level L1. For example, the maximum output power for the top panel in Conc-A for this level (L2) at solar noon time is 9.1 W, whereas it was ~12.8 W for Level L1 for the same concentrator and at the same time. These values for Conc-B were 8.5 W for L2 and 12.7 W for L1. In fact, lower power values are recorded for both the top panel and the back panels at all times of the day.

The output of the top panel being less is reasonable because as the receiver location becomes closer to the top of the concentrator, less reflected radiation will be received by this panel. For the back panel, it was expected that the back panel would receive more reflected radiation, yet the collected power would increase as the panel moves up to the surface of the concentrator. However, the collected data showed the opposite results, where

the output of this panel decreased when it moved up. This can be attributed to the fact that as the back panel moves up, the capture factor becomes smaller and smaller, and hence more radiation misses the back panel.

Another set of data was taken for the systems under study when the receiver panels are located at the top of the concentrator opening, L3. In this situation, the top panel in both concentrators will receive only direct radiation, while the back panel receives reflected radiation, as in other situations, but here it is expected to receive greater radiation compared to other positions L1 and L2. The results of the measurements are shown in Figs 16 and 17 for the two concentrators. As can be seen from the figures, the *I*–*V* and *P*–*V* curves for the top panel in both concentrators overlay each other, as expected. The output power and current from the panels in the back of concentrators are lower than what is expected since, in this case, the area of walls under the panel that reflects radiation is the whole area of the wall. This behaviour of the panels in the back can be connected to the assumption that the capture factor becomes smaller and hence much more radiation misses the panels in the back.

When the power generated by the back panel and the top panel for the two concentrators at different times of the day is compared, one can see that the ratio of maximum power generated by the back panel to that generated by the top panel has the smallest ratio at early times of the day, and the value of this ratio increases by the time it reaches its maximum value at noon. Table 1 shows

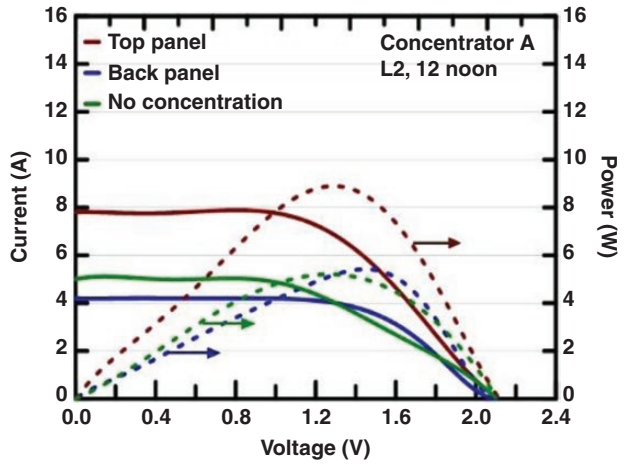

Fig. 14: *I*–*V* and *P*–*V* curves for Conc-A, L2, 12:00 noon, 18 October 2018.

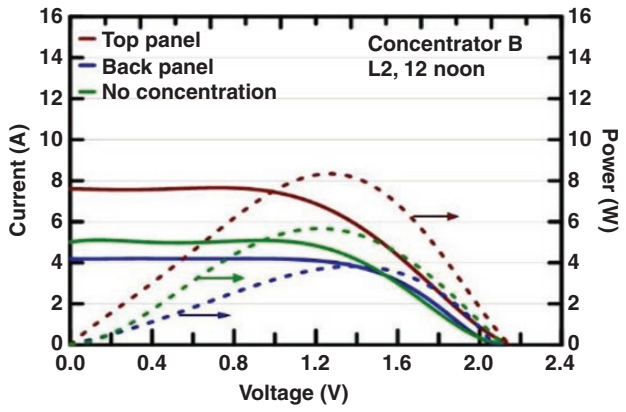

Fig. 15: *I*–*V* and *P*–*V* curves for Conc-B, L2, 12:00 noon, 18 October 2018.

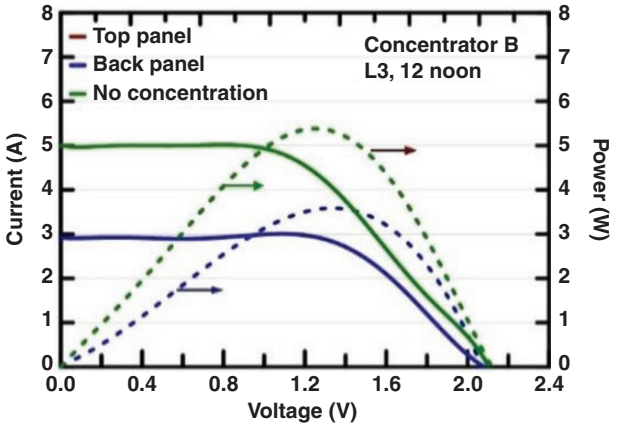

Fig. 16: *I*–*V* and *P*–*V* curves for Conc-B, L3, 12:00 noon, 19 October 2018.

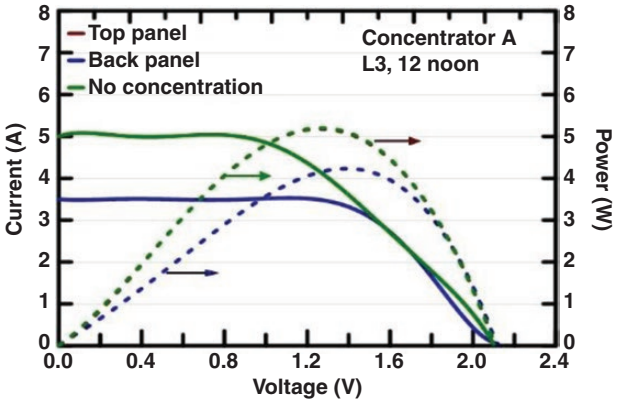

Fig. 17: *I*–*V* and *P*–*V* curves for Conc-A, L3, 12:00 noon, 19 October 2018.

Table 1: Ratio of power generated by back panel to that generated by top panel at different levels and times

$\frac{(Ppm)back}{(Ppm)top}$	PV panel position	Concentrator	8:00 a.m.	10:00 a.m.	12:00 (noon)
	L1	A	25%	32%	52%
		B	22%	33%	46%
	L2	A	32%	46%	57%
		B	25%	27%	24%
	L3	A	44%	58%	68%
		B	35%	32%	61%

the values of the ratio for both concentrators. This shows that, at around noon, more radiation from the top panel is reflected to the back panel, and hence the ratio increases with time.

The values for afternoon times are similar to the corresponding times before noon. It can be seen that the value of this ratio is higher for Conc-A for all levels of panels inside the concentrators.

When the total power collected by the two concentrators for all three levels is compared (Fig. 18), the results clearly show that the best location for the PV receiving panels is the lowest level inside the concentrator (L1).

Using the following equation [46], the electrical efficiency of the two concentrators was calculated for the three levels at solar noon:

$$\eta_{El} = \frac{P_T}{G\,A_a} \tag{6}$$

where P_T is the total output power of the concentrator, G is the radiation density on the surface of the concentrator and A_a is the aperture area. The calculated electrical efficiency of the three configurations is shown in Table 2. Clearly the efficiency at around noon is higher than that at other times of the day, and the L1 arrangement has the highest electrical efficiency, followed by the L2 and L3 arrangements.

4 Conclusion

This paper proposes two LCPV concentrators, each of which consists of two components. The bottom component (common to both concentrators) is composed of two adjacent parabolas, whereas the side component (wall) may be either flat or paraboloid (Fig. 6). Using Ray Optics Simulation Software, the concentrators are designed to reflect solar radiation towards a bifacial solar PV panel that accepts radiation from both sides. The theoretical geometrical CR and the effective CR were, respectively, 3.83 and 3.23. The two concentrators are examined in open air, leading to the following conclusions:

(i) Throughout the day, the electrical efficiency of the concentrators fluctuated between 8.3% and 18.2%.
(ii) Conc-A with flat reflecting walls exceeded Conc-B with paraboloid reflecting walls (with corresponding average C_{eff} values of 1.98 and 1.81).
(iii) At midday, the maximum value for C_{eff} was measured to be ~3.1, which was close to its theoretical value of 3.23.
(iv) The optimal placement of the receiver within both concentrators was determined to be at the lowest level, L1, and the worst was at the third highest level, L3 (Fig. 7).

As a continuation of the current work, it is suggested that additional research be conducted to investigate the effects of optical flux distributions on concentrator efficiency and to develop a method for predicting solar cell temperature and determining the impact of temperature on solar cell performance.

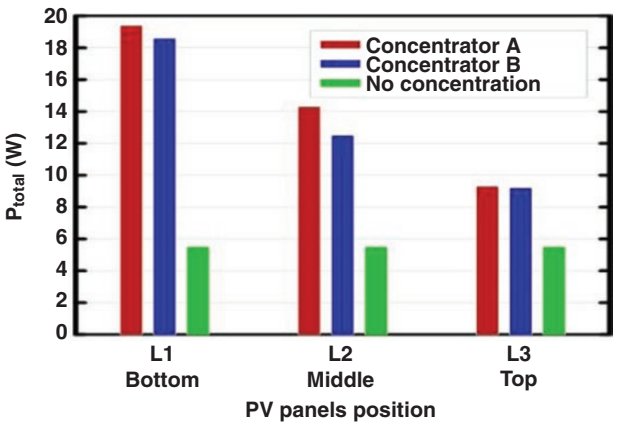

Fig. 18: Amount of power generated by front and rear modules in each arrangement.

Nomenclature

A_a:	aperture area of the concentrator
A_r:	receiver area
C_{eff}:	effective concentration ratio
C_g:	geometric concentration ratio
C_{opt}:	optical concentration ratio
FF:	fill factor
G:	radiation density on the aperture of the concentrator
$(P_{pm})_{back}$:	output power of panel in the bottom
$(P_{pm})_{top}$:	output power of panel in top
P_T:	total power
R:	reflectance of the reflectors
α:	incident angle
θ:	acceptance angle
η_{El}:	electrical efficiency

Table 2: Electrical efficiency of concentrators throughout the day for each arrangement

Time	Electrical efficiency					
	Concentrator A			Concentrator B		
	L1	L2	L3	L1	L2	L3
8:00	16.1%	14.8%	15.1%	12.2%	12.1%	11.5%
9:00	17.4%	15.4%	15.0%	13.7%	12.3%	9.9%
10:00	17.9%	16.1%	16.0%	14.4%	11.3%	9.3%
11:00	17.8%	16.8%	14.4%	12.5%	12.6%	10.2%
12:00	18.2%	17.6%	14.1%	11.6%	11.8%	11.4%
13:00	16.8%	17.1%	12.5%	12.0%	10.8%	10.1%
14:00	15.8%	14.3%	11.8%	11.9%	9.0%	8.0%
15:00	14.4%	14.2%	11.3%	11.7%	8.7%	8.2%
16:00	11.2%	11.2%	8.7%	10.0%	8.5%	8.3%

Acknowledgements

The authors would like to thank the Solar Energy Lab at the physics department for allowing us to utilize the Lab's tools and facilities.

Funding

This research received no funding.

Conflict of interest statement

The authors have no competing interests to declare that are relevant to the content of this article.

References

[1] International Energy Agency. *Global Energy Review*. 2021. https://iea.blob.core.windows.net/assets/d0031107-401d-4a2f-a48b-9eed19457335/GlobalEnergyReview2021.pdf (1 March 2023, date last accessed).

[2] Green MA. How did solar cells get so cheap? *Joule*, 2019, 3:631–633.

[3] Feldman D, Ramasamy V, Fu R, *et al*. *US Solar Photovoltaic System and Energy Storage Cost Benchmark (Q1 2020)*. Golden, CO: National Renewable Energy Lab (NREL), 2021.

[4] Lee D-K, Park N-G. Materials and methods for high-efficiency perovskite solar modules. *Solar RRL*, 2022, 6:2100455.

[5] Zhao X, Liu T, Burlingame QC, *et al*. Accelerated aging of all-inorganic, interface-stabilized perovskite solar cells. *Science*, 2022, 377:307–310.

[6] France RM, Geisz JF, Song T, *et al*. Triple-junction solar cells with 39.5% terrestrial and 34.2% space efficiency enabled by thick quantum well superlattices. *Joule*, 2022, 6:1121–1135.

[7] Romaní J, Ramos A, Salom J. Review of transparent and semi-transparent building-integrated photovoltaics for fenestration application modeling in building simulations. *Energies*, 2022, 15:3286.

[8] Tarancón A, Esposito V, Torrell M, *et al*. 2022 roadmap on 3D printing for energy. *J Phys: Energy*. 2022, 4:011501.

[9] Deline C, MacAlpine S, Marion B, *et al*. Evaluation and field assessment of bifacial photovoltaic module power rating methodologies. In: *2016 IEEE 43rd Photovoltaic Specialists Conference (PVSC)*, Portland, OR, USA, 5–10 June 2016, 3698–3703.

[10] Pérez-Higueras P, Ferrer-Rodríguez JP, Almonacid F, *et al*. Efficiency and acceptance angle of high concentrator photovoltaic modules: current status and indoor measurements. *Renew Sustain Energy Rev*, 2018, 94:143–153.

[11] Alamoudi A, Saaduddin SM, Munir AB, *et al*. Using static concentrator technology to achieve global energy goal. *Sustainability*, 2019, 11:3056.

[12] Benhammane M, Notton G, Pichenot G, *et al*. Overview of electrical power models for concentrated photovoltaic systems and development of a new operational model with easily accessible inputs. *Renew Sustain Energy Rev*, 2021, 135:110221.

[13] Amanlou Y, Hashjin TT, Ghobadian B, *et al*. A comprehensive review of uniform solar illumination at low concentration photovoltaic (LCPV) systems. *Renew Sustain Energy Rev*, 2016, 60:1430–1441.

[14] Freier D, Ramirez-Iniguez R, Jafry T, *et al*. A review of optical concentrators for portable solar photovoltaic systems for developing countries. *Renew Sustain Energy Rev*, 2018, 90:957–968.

[15] Shanks K, Senthilarasu S, Mallick TK. Optics for concentrating photovoltaics: trends, limits and opportunities for materials and design. *Renew Sustain Energy Rev*, 2016, 60:394–407.

[16] Paul DI. Application of compound parabolic concentrators to solar photovoltaic conversion: a comprehensive review. *Int J Energy Res*, 2019, 43:4003–4050.

[17] Jaaz AH, Hasan HA, Sopian K, *et al*. Design and development of compound parabolic concentrating for photovoltaic solar collector. *Renew Sustain Energy Rev*, 2017, 76:1108–1121.

[18] Parupudi RV, Singh H, Kolokotroni M, *et al*. Long term performance analysis of low concentrating photovoltaic (LCPV) systems for building retrofit. *Appl Energy*, 2021, 300:117412.

[19] Alnajideen M, Gao M. A new configuration of V-trough concentrator for achieving improved concentration ratio of > 3.0 x. *Sol Energy Mater Sol Cells*, 2022, 245:111877.

[20] Butler B, Van Dyk E, Vorster F, *et al*. Characterization of a low concentrator photovoltaics module. *Physica B*, 2012, 407:1501–1504.

[21] Khamooshi M, Salati H, Egelioglu F, *et al*. A review of solar photovoltaic concentrators. *Int J Photoenergy*, 2014, 2014:1958521–1958517.

[22] Mallick T, Eames P, Hyde T, *et al*. The design and experimental characterisation of an asymmetric compound parabolic photovoltaic concentrator for building façade integration in the UK. *Sol Energy*, 2004, 77:319–327.

[23] Mokri A, Emziane M. Concentrator photovoltaic technologies and market: a critical review. In: *World Renewable Energy Congress-Sweden*, Linköping, Sweden, 8–13 May 2011, 2738–2742.

[24] Zhang H, Chen H, Liu H, *et al*. Design and performance study of a low concentration photovoltaic-thermal module. *Int J Energy Res*, 2018, 42:2199–2212.

[25] Zhang H, Liang K, Chen H, *et al*. Thermal and electrical performance of low-concentrating PV/T and flat-plate PV/T systems: a comparative study. *Energy*, 2019, 177:66–76.

[26] Masood F, Nor NBM, Nallagownden P, *et al*. A review of recent developments and applications of compound parabolic concentrator-based hybrid solar photovoltaic/thermal collectors. *Sustainability*, 2022, 14:5529.

[27] Katardjiev I. A fractal concentrator of direct and indirect sunlight. *Clean Energy*, 2020, 4:305–315.

[28] Stein J, Hansen C, Deline C, *et al*. *Comparison of Modeling Methods and Tools for Bifacial PV Performance*. Albuquerque, NM: Sandia National Lab.(SNL-NM), 2017.

[29] Martin PJ, Tamizhmani G. Optimization of back reflectors for bifacial photovoltaic modules. In: *2019 IEEE 46th Photovoltaic Specialists Conference (PVSC)*, Chicago, IL, USA, 16–21 June 2019, 0526–0531.

[30] Yusufoglu UA, Pletzer TM, Koduvelikulathu LJ, *et al*. Analysis of the annual performance of bifacial modules and optimization methods. *IEEE J Photovoltaics*, 2014, 5:320–328.

[31] Cha HL, Bhang BG, Park SY, *et al*. Power prediction of bifacial Si PV module with different reflection conditions on rooftop. *Applied Sciences*, 2018, 8:1752.

[32] Rabl A. Comparison of solar concentrators. *Sol Energy*, 1976, 18:93–111.

[33] Chacin L, Rangel S, Cabral D, *et al*. Impact study of operating temperatures and cell layout under different concentration factors in a CPC-PV solar collector in combination with a vertical glass receiver composed by bifacial cells. In: *SWC/SHC 2019 Solar World Congress*, Santiago, Chile, 4–7 November 2019.

[34] Panchal R, Gomes J, Cabral D, *et al*. Evaluation of symmetric C-PVT solar collector designs with vertical bifacial receivers.

In: *SWC/SHC 2019 Solar World Congress*, Santiago, Chile, 4–7 November 2019, 165–176.

[35] Poulek V, Khudysh A, Libra M. Innovative low concentration PV systems with bifacial solar panels. *Sol Energy*, 2015, 120:113–116.

[36] Aghaei M, Pelosi R, Wong WW, *et al*. Measured power conversion efficiencies of bifacial luminescent solar concentrator photovoltaic devices of the mosaic series. *Prog Photovolt Res Appl*, 2022, 30:726–739.

[37] Welford WT, Winston R. *Optics of Nonimaging Concentrators: Light and Solar Energy*. New York: Academic Press, 1978.

[38] Winston R, Miñano JC, Benitez PG. *Nonimaging Optics*. Burlington, MA: Elsevier Acadenic Press, 2005.

[39] Stine WB, Geyer M. Power from the Sun. 2001. https://www.powerfromthesun.net/book.html (7 November 2022, date last accessed).

[40] Al-Najideen M, Al-Shidhani M, Min G. Optimum design of V-trough solar concentrator for photovoltaic applications. *AIP Conf Proc*, 2019, 2149:030001.

[41] Johnson TR, and Cheng S. Ray optics simulation. https://ricktu288.github.io/ray-optics/simulator/ (7 November 2022, date last accessed).

[42] Gu X, Taylor RA, Morrison G, *et al*. Theoretical analysis of a novel, portable, CPC-based solar thermal collector for methanol reforming. *Appl Energy*, 2014, 119:467–475.

[43] Abd HM, Alomar OR, Ali FA, *et al*. Experimental study of compound parabolic concentrator with flat plate receiver. *Appl Therm Eng*, 2020, 166:114678.

[44] Cabral D, Gomes J, Karlsson B. Performance evaluation of non-uniform illumination on a transverse bifacial PVT receiver in combination with a CPC geometry. *Sol Energy*, 2019, 194:696–708.

[45] Cabral D. Development and performance comparison of a modified glazed CPC hybrid solar collector coupled with a bifacial PVT receiver. *Appl Energy*, 2022, 325:119653.

[46] Shakouri M, Ebadi H, Gorjian S. Solar photovoltaic thermal (PVT) module technologies. In: Gorjian S, Shukla A (eds). *Photovoltaic Solar Energy Conversion*. London: Elsevier Academic Press, 2020, 79–116.